Systematic Mn d-configuration change in the $La_{1-x}Ca_xMnO_3$ system: A Mn K-edge XAS study

M. Croft and D. Sills
Department of Physics, Rutgers University, Piscataway, New Jersey 08855

M. Greenblatt and C. Lee
Department of Chemistry, Rutgers University, Piscataway, New Jersey 08855

S.-W. Cheong
Bell Laboratories, Lucent Technologies, Murry Hill, New Jersey 07974

K. V. Ramanujachary and D. Tran
Department of Chemistry and Physics, Rowan College of New Jersey, Glassboro, New Jersey 08028-1701

(Received 3 October 1996)

Systematic Mn K-edge x-ray-absorption spectroscopy (XAS) measurements on samples of $La_{1-x}Ca_xMnO_3$ are reported. Detailed results on the chemical shift and pre-edge feature spectral strength (both indicators of the Mn d-hole count) are discussed. The overall chemical shift across the series is compared to standard materials and is consistent with the identification of the endpoint perovskites with the Mn^{3+} and Mn^{4+} states. The detailed compositional dependence of the chemical shift and the strength of the pre-edge feature both indicate a uniform Ca-induced increase in the Mn d-hole count for $x>0.2$ and an anomalous break from this behavior for x values less than $x\approx 0.2$. Careful x-ray-diffraction measurements of the lattice parameter variation are also found to manifest changes near $x\approx 0.2$ and the chemical shift results are shown to scale with the lattice parameter results. Additional XAS results on air prepared and oxygen annealed samples reveal a variation in the chemical shift response to excess oxygen across this series. These XAS results are discussed in terms of the important Mn d-hole count variation across this system. [S0163-1829(97)04114-3]

INTRODUCTION

The $La_{1-x}A_xMnO_3$ system, with A=Ca, Sr, Ba, and Pb, exhibit a host of interesting physical phenomena, including insulator-to-metal transitions, the crossover from antiferromagnetic to ferromagnetic (FM) order, and the recently identified occurrence of charge ordering transitions.[1–4] In the composition regime where the ferromagnetic ordering and insulator-metal transitions are coupled, the occurrence of ''colossal'' magnetoresistance has also been of great interest for technological applications.[4] Theoretical modeling of all of these effects (such as the double-exchange-induced FM interactions[5] or the local Jahn-Teller contributions to the magnetoresistance[6]) involve the crucial assumption of a formal Mn^{3+} d^4, to Mn^{4+} d^3 configurational change with the A^{2+} substitution. Consequently the development of a systematic experimental understanding of the Mn-configuration variation in these materials is also crucial.

The importance of chronicling experimentally the Mn-configuration variation in these materials is emphasized by experience in high-T_c Cu-oxide materials. Namely, similar types of substitution (e.g., A^{2+} for La^{3+}) in those materials often proved to dominantly induce holes of O p character rather than to vary the formal Cu d occupancy.[10] Thus in such transition-metal materials the d character of the doped holes should be considered carefully for each system.

In the past, transition-metal (T) K-edge x-ray-absorption spectroscopy (XAS) measurements have proved to be a useful tool in identifying the T-configuration changes and d-hole character in such oxide compounds.[11–13] In this paper a detailed Mn K-edge XAS study is presented for the $La_{1-x}Ca_xMnO_3$ system. In particular the chemical shift of the Mn K-edge and the spectral intensity of a pre-edge feature (involving d states) will be shown to evidence strong d-hole count changes in this system. While the detailed x dependence of the XAS results exhibit a strong linear x dependence for $x>0.2$, a break in behavior for lower compositions is observed. This break is interpreted in terms of a differing Mn d-hole response to Ca substitution. The XAS results are shown to be well correlated with the structural results on this system. Finally the Mn-site response of these materials to increased relative O content is discussed. Before proceeding a brief review of previous results addressing the Mn electronic configuration in these materials will be made.

PREVIOUS Mn-CONFIGURATION RESULTS

The longest standing indicator of the large Mn-configuration change in these $La_{1-x}A_xMnO_3$ materials is from wet chemical titration techniques. Titration measurements, on the dissolved compounds, have been used, over a number of years, to show the increase of the formal Mn^{4+} fraction upon A^{2+} substitution in these systems.[7,8] Recently, Mahendiran *et al.*[9] have used the titration method to correlate the Mn^{4+} percentage with the structural, magnetic, and transport properties of $(La,A)MnO_3$ [A=Ca and Sr] materials. Their work emphasized a number of points, along which were the role of metal site vacancies with varying O content;

 © 1997 The American Physical Society

the orthorhombic-to-rhombohedral-to-cubic structure change associated with increasing Mn^{4+} fraction; and finally the variation of the magnetic response to the Mn^{4+} percentage.[9] Their work clearly motivates the need to establish a clear linkage between the titration techniques and spectroscopic probes of the Mn d-hole count variation in these materials.

Spectroscopic studies have also been applied to various compounds in this class of Mn perovskites. Abbate *et al.*[15] performed soft x-ray-absorption spectroscopy (SXAS) on the Mn $L_{2,3}$ edges (640–655 eV) and the O K edges (530 eV) of selected A=Sr materials. They inferred a basically Mn d^4 configuration at $x=0$ and a d^3-$d^4\underline{L}$ admixture at $x=0.9$. (Here the $\underline{L}$ denotes an O-ligand hole.) The study of Saitoh *et al.*[16] extended this work on the A=Sr system by combining photoemission results with the SXAS. This latter work concluded the Mn configurations to be 50% d^4/40% $d^5\underline{L}$/10% $d^6\underline{L}^2$ at $x=0$ and 40% d^3/50% $d^4\underline{L}$/10% $d^5\underline{L}^2$ at $x=0.9$, with a net d-hole count change across the series of about $0.7e^-$.[16] As will become evident from the results presented below, one minor point in the work of Saitoh *et al.*[16] is also worth noting: with increasing x the Mn $2p_{3/2}$ core level manifested a binding energy decrease in the $0<x<0.3$ range followed by an increase in the $0.3<x<0.9$ range. The former decrease was attributed to the Fermi energy (E_F) shift (accompanying the insulator-metal transition) while the latter increase was ascribed to the more conventional chemical shift with increasing Mn valence.

Sarma *et al.*[17] reported O K-edge SXAS results on A=Sr materials similar to those reported by Abbate *et al.*[15] However, the work of Sarma *et al.* involved more closely spaced compositions with $x<0.5$. By subtracting the $x=0$ spectrum from those of the higher concentrations they noted, that there was no change in the above-E_F states between $x=0$ and $x=0.1$, but that there was a uniform enhancement in these states for $x>0.2$. Again the notion of a depressed, low-x behavior will be echoed by the results presented below.

Recently Park *et al.*[18] reported photoemission and O K-SXAS measurements on the A=Ca system. Their work, while consistent with a charge fluctuation gap for Mn^{3+}-site to Mn^{4+}-site hopping in the high-temperature paramagnetic phase, confirmed metallic states below E_F in the low-temperature FM phase. In addition to inferring a number of the d-configuration energy parameters, they also concluded that the materials in this system were strongly and inhomogeneously mixed (Mn^{3+}/Mn^{4+}) valent across the entire series.

Thus there is already evidence for a significant Mn-valence and Mn d-hole count increase accompanying various A substitutions into $LaMnO_3$. A detailed spectroscopic picture of the Mn-configuration variation across a given series is however lacking. The present XAS study contributes to such a picture for the A=Ca system. Moreover the results presented here indicate that the Mn K-XAS technique is both sensitive and flexible enough to extend comparison of the Mn-configuration response to various A substitutes, upon thin-film formation, and in various generalizations to layered perovskite structures.

The previous spectroscopic work has emphasized that the formal Mn^{3+} (Mn^{4+}) states in these materials do not correspond to pure ionic $3d^4$ ($3d^3$) states. Very substantial covalent admixing, of the Mn d configurations, will be involved in the perovskite and standard materials discussed in this paper. Nevertheless the XAS techniques used in this paper are sensitive to the detailed, relative variation in the d-hole count in these admixed states.

EXPERIMENTAL

The samples from Bell Labs, Lucent Technologies were prepared by standard solid-state reactions in air as described previously.[1] The synthesis of the $La_{1-x}Ca_xMnO_3$ materials at Rutgers was carried out using a coprecipitation technique.[19] Stoichiometric amounts of rare-earth sesquioxide (preheated to remove water and carbon dioxide) and alkaline earth nitrate were dissolved in nitric acid. A stoichiometric amount of manganese (II) nitrate solution was then added and the mixed metals were precipitated, as carbonates, using ammonium carbonate. The solution with the precipitate was aged at $\sim$50 °C for 6–8 h. The precipitate was subsequently recovered by filtration and heated, in air, to 1100 °C for 24 h with intermediate grindings performed for homogeneity.

X-ray powder-diffraction measurements, made with an automated SCINTAG diffractometer, were used to verify that the materials were single phase utilizing comparison with literature (JCPDS) profiles. The lattice parameters were obtained by least-squares fitting over $10°<2\Theta<80°$ using an internal standard. The diffraction patterns of many of the materials were indexed both according to the cubic and rhombohedral structures. However, within the 2θ range analyzed and within the diffractometer resolution no deviations from the cubic structure were perceivable for $x>0.2$. For $x<0.2$ the rhombohedral indexing proved superior. This structure crossover is consistent with that reported by Mahesh and co-workers.[24,25]

The XAS measurements were made in the electron yield and fluorescence modes[20,21] on beam line X-19A at the Brookhaven National Synchrotron Light Source using, a double crystal [Si(200) or Si(311)] monochromator. Transmission mode XAS measurements were made simultaneously confirming the results of the other modes. A standard was run simultaneously with all measurements for precise calibration. The relative energies between various spectra was established by careful comparison of the standard spectra. Particular care was taken to use the identical standard sample maintained in a constant position to accurately calibrate the chemical shift results. In general the relative accuracy of the energy is about ± 0.05 eV. The absolute energy of the spectra is pinned to the first inflection point of pure Mn (6539.0 eV) and to the main peak of MnO (6555.0) eV. All spectra were normalized to unity step in the absorption coefficient from well below to well above the edge.

Mn STANDARDS AND (La, Ca)MnO_3 CHEMICAL SHIFTS

In Fig. 1 the Mn K-edge spectra for the series of Mn^{n+} ($n=0$, 2, 3, 4, and 7) standards, Mn, MnO, Mn_2O_3,

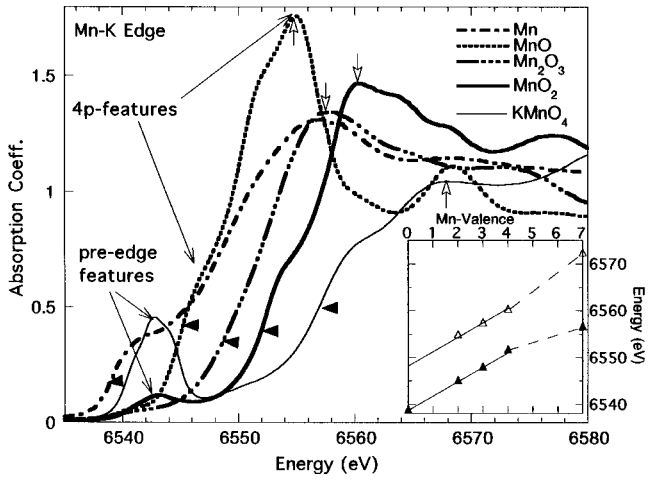

FIG. 1. The Mn *K*-edge spectra (absorption coefficient, μ, versus photon energy) for the series of Mn^{n+} ($n=0$, 2, 3, 4, and 7) standards, Mn, MnO, Mn_2O_3, MnO_2, and $KMnO_4$. The dark arrow heads indicate the first inflection point at the main edge traditionally used to define the chemical shift. The open arrows indicate the energy of the peak at the edges of the oxide standards. Selected $4p$ features for MnO and the pre-edge (Mn *d* related) features of MnO_2 and $KMnO_4$ are indicated. (inset) The chemical shift of the standard Mn compounds (solid triangles) versus the formal Mn valence. Also plotted in the inset are the energies of the peaks (open triangles) of the oxide standards.

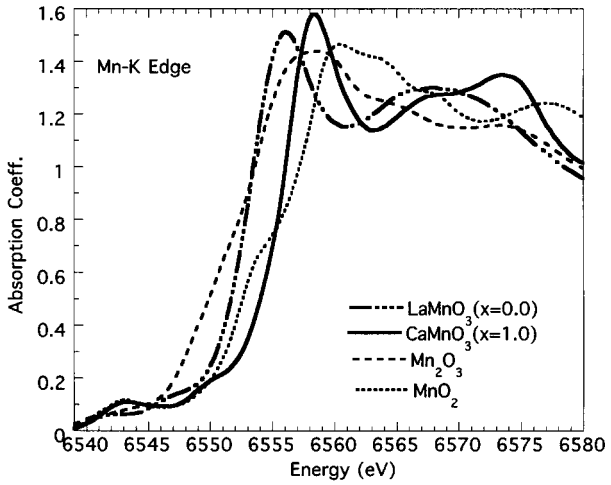

FIG. 2. The Mn *K*-edge spectra for the $x=0.0$ and $x=1.0$ end-point compounds in the $La_{1-x}Ca_xMnO_3$ series, along with those of the Mn_2O_3 and MnO_2 standards. Note the perovskite spectra lie in energy intermediate between the shoulder and peak $4p$ features of the analogous Mn^{3+} and Mn^{4+} standards.

MnO_2, and $KMnO_4$, are shown. It is clear from the figure that there is a substantial chemical shift of the edge with increasing formal chemical valence. As noted earlier, covalency will hybridize different $3d$ configurations into the ground state of each of these integral valent standards. However, the increase *d*-hole count with increasing formal valence will be large enough to outweigh these covalency effects. Since the creation of holes in the rather localized *d* orbitals contributes strongly to the chemical shift (by loss of screening) this strong chemical shift in the Mn standards is reflective of the substantial increase in the Mn *d*-hole count in the higher-valence-state compounds. The first inflection point of the main edge is often used[22] to define the chemical shift and these points are indicated by the dark arrow heads (on the spectra) in the figure. The chemical shifts (defined by these inflection points) of the edges are plotted versus the formal chemical valence in the inset of Fig. 1.

Despite the orderly valence-shift correlation for these standards, the strong spectral features at the edges complicate the generalization of a simple chemical shift definition to all Mn compounds. Therefore some consideration of these near-edge spectral features must be made. The main feature at the Mn *K* edge is an absorption step associated with the onset of core-level ($1s$) to continuum transitions. This feature, however, lies unresolved beneath a number of overlapping spectral peaks and will not be of import here. Atomic-like transitions from the $1s$ core to empty $4p$ states also produce multiple peaks in the near-edge energy region. The multiplicity of these features is governed by the solid-state splittings of the $4p$ levels and by replication of $4p$ features associated with different $3d$ configurations (see two of the $4p$ features of MnO indicated in Fig. 1 for example).[23] Finally there is a pre-edge feature (split about 7 eV below the main edge rise) caused by $1s$ electron transitions into empty *d* states, or hybridized d/p states (see the prominent *d*-pre-edge features of MnO_2 and $KMnO_4$ indicated in Fig. 1, for example).[23]

In assigning a chemical shift for an edge the splitting of the $4p$ features should be kept in mind. Using the first inflection point of the main edge definition defines the edge essentially by the lowest energy $4p$ feature. In the $La_{2-x}Sr_xNiO_4$ system, for example, the initial edge onset is dominated by the variation of the energy of the out-of-plane, Ni $4p_\pi$ state.[13] The main peak at the Mn *K* edge of these oxide compounds (see the open headed arrows in Fig. 1) corresponds to another of the higher energy $4p$ features. As the Mn valence increases the centroid of the split $4p$ features shifts up in energy. In the inset of Fig. 1 the energy of the peak $4p$ feature is also plotted for the oxide compounds. The solid lines in the inset are parallel, indicating that the low-energy $4p$ feature (identified by the inflection-point energy) and the peak-$4p$-feature track one another with increasing Mn valence. The divergence of the two features for $KMnO_4$ presumably reflects the influence of an increased $4p$ splitting.[23]

Unlike the binary oxides (where the $4p$ oscillator strength is spread comparably over several split features) in the perovskite compounds of interest here most of the spectral strength lies in the main $4p$ feature at the edge. This is illustrated in Fig. 2 where the spectra of $LaMnO_3$ and $CaMnO_3$ are compared to those of Mn_2O_3 and MnO_2. It should be noted that the main $4p$ peaks for the La-Mn^{3+} perovskite and for the Ca-Mn^{4+} perovskite lie, respectively, intermediate between lower and higher $4p$ features of the Mn^{3+} and Mn^{4+} binary oxides. This intermediate positioning supports the basically Mn^{3+} and Mn^{4+} identification of the end-point perovskite compounds. For these perovskites the energy value of the intense $4p$ peak at the edge provides a convenient reference to track the relative chemical shifts

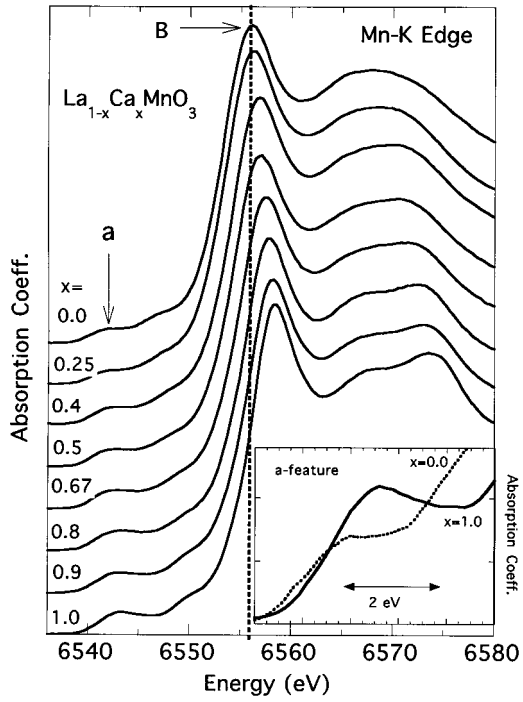

FIG. 3. Illustration of the evolution of the Mn K-edge spectra with x in the $La_{1-x}Ca_xMnO_3$ series. The dashed vertical line, passing through the peak of the $x=0$ spectrum, serves as a reference to emphasize the uniform shift of this B-feature peak with x. Note also the enhancement of the pre-edge a feature with increasing x. (Inset) An enlargement of the pre-edge a-feature region clarifying the large enhancement of the a-feature intensity and showing its absolute energy shift between $x=0$ (dashed line) and $x=1$ (solid line).

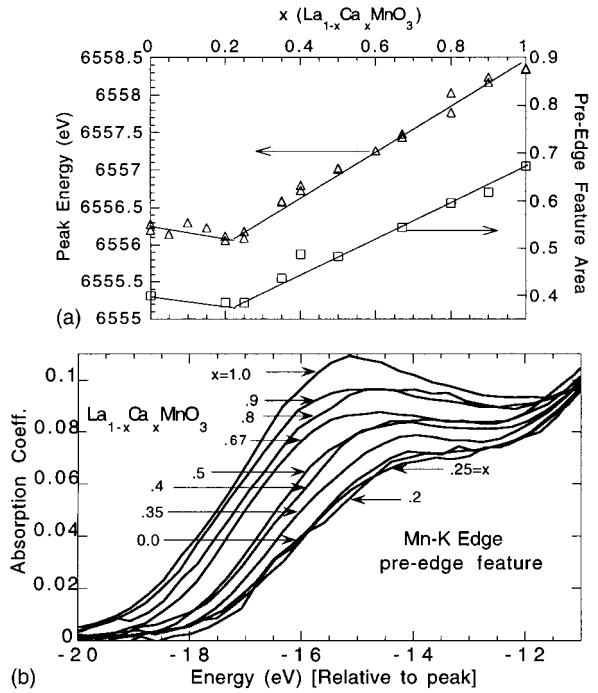

FIG. 4. (a) (top) The energy of the B-feature spectral peak in the $La_{1-x}Ca_xMnO_3$ series (left scale) versus x. Note the near linear increase for $x>0.2$ and the break from this behavior for $x<0.2$. Also, the integrated spectral area (right scale) in the region of the pre-edge a features for the $La_{1-x}Ca_xMnO_3$ series. The a-feature integration limits used were from -20 to -11 eV with the zero of energy set at the B-feature peak [as in (b)]. (b) (bottom) The pre-edge a features in the $La_{1-x}Ca_xMnO_3$ series. The zero of energy for all of the spectra has been set at the B-feature peak.

and will be so used throughout the rest of this paper.

Although the differing $4p$-feature structures prevent clear direct comparison of the chemical shifts between the perovskites and the standards, it is possible to examine the magnitude of the shift across the $La_{1-x}Ca_xMnO_3$ series. The magnitude of the shift between $LaMnO_3$ and $CaMnO_3$ is about 70% as large as that between the Mn_2O_3 and MnO_2 standards. Although the clear identification of the Mn d count in the strongly hybridized standards is questionable, if one assumes integral change in the Mn d-hole count between the Mn^{3+} and Mn^{4+} standards, then the net d-hole count change in the perovskite series is relatively about $0.7e^-$. This estimate is consistent with the estimate of Saitoh *et al.*[16] for the end-point compounds.

$La_{1-x}Ca_xMnO_3$ CHEMICAL SHIFT

In Fig. 3 the evolution, with x, of the Mn K-edge spectra for the $La_{1-x}Ca_xMnO_3$ series of compounds is shown. It should be noted that there is a systematic shift of the edges to higher energy with increasing x. The energy of the main peak at the edge (labeled B in the figure) is used to follow this shift, as underscored by the peak shift relative to the dotted line passing through the B peak of the $x=0$ spectrum. The detailed x variation of these peak energies is presented in Fig. 4(a) (left scale). Comparison of the right scale results to these shift results will be differed. For $x>0.2$ the edge shift is seen to increase nearly linearly, within the errors, with increasing x. Extrapolation of this monatomic behavior breaks down between $x=0.0$ and $x=0.2$, where the peak shifts down slightly in energy with increasing x. Note that the finer grid of compositions with $x<0.2$ unambiguously confirms this anomalous break in the shift variation.

$La_{1-x}Ca_xMnO_3$ PRE-EDGE FEATURE VARIATION

As noted above, for the standard compound spectra, the small pre-edge a feature, in the spectra of Fig. 3, is associated with transitions involving empty Mn $3d$ final states. Both quadrupole allowed $1s$ to $3d$ and dipole allowed $1s$ to $4p$ states (hybridized with the Mn $3d$ states) can contribute to this feature.[12–14] Increasing spectral weight of this pre-edge feature (within a given symmetry environment) is typically associated with an increasing d-hole count in $3d$ transition-metal compounds.[12–14] Inspection of Fig. 3 reveals a substantial enhancement of this a feature with increasing x. In Fig. 4(b) the detailed Mn K-pre-edge feature variation, across the $La_{1-x}Ca_xMnO_3$ series, is illustrated on an expanded energy scale. For clarity of comparison the zero of energy in Fig. 4(b) has been chosen at the main B peak (the relation of the $x=0$ and $x=1$ a features, on an absolute

energy scale, is illustrated in the inset of Fig. 3). The dramatic enhancement of the pre-edge *a* feature across the series is clear from Fig. 4(b).

To quantify this enhancement the spectra of Fig. 4(b) have been integrated over the energy range of -20 to -11 eV. These areas are plotted versus x in Fig. 4(a) (right scale). This pre-edge area variation shows little or no response for $x<0.2$, but increases strongly and nearly linearly with x for $x>0.2$. This is, of course, strikingly similar to the chemical shift variation with x shown in the same figure. It should be noted that determination of the absolute *a*-feature area would be dependent on the choice of the strongly varying background in this energy range and is therefore not attempted here. Nevertheless, this area enhancement is such that background issues are not important for qualitative conclusions. Namely the clear inferences from the pre-edge *a*-feature variation are that the Mn *d*-hole count, and the Mn *d*/*p* hybridization (above the Fermi energy) increases substantially with x in this series; and that there is apparently an anomalous lack of the Mn *d* response to Ca substitution for $x<0.2$ in this series.

$La_{1-x}Ca_xMnO_3$ STRUCTURE XAS CORRELATION

Thus, for this class of air synthesized $La_{1-x}Ca_xMnO_3$ materials, both the chemical shift and the pre-edge feature strength changes are mutually consistent with a large Mn *d*-hole count increase with Ca substitution. Interestingly, however, these results also concur in a nonuniform x dependence in the Mn *d*-hole count for smaller x values. With these results in mind a careful x-ray-diffraction study of the structural properties of these materials was performed. The results of this study are presented in Table I. In order to compare the lattice variation across the rhombohedral-cubic transformation the cube root of the unit-cell volume per formula unit (a_p) has been calculated.[26,27] The a_p represents an estimate of the effective perovskite unit-cell parameter. In Fig. 5(a) a_p is plotted versus x for the $La_{1-x}Ca_xMnO_3$ system. The first point to note is that the lattice parameter results manifest a break in behavior near $x=0.2$. The rhombohedral and cubic phase results of Mahesh *et al.*[24,25] agree well (when similarly plotted) with those of this study, including the structural break near $x=0.2$. Comparison of lattice parameter results obtained by both cubic and rhombohedral indexing for $0.0<x<0.5$ verified that the break in a_p was not simply due to the structure indexing scheme.

Motivated by the similar x dependences of the structural and XAS results the Mn *K*-edge peak positions are plotted versus the effective perovskite lattice parameter in Fig. 5(b). Within the experimental uncertainties the correlation of the lattice parameter to the Mn *K*-edge shift (and thereby presumably to the Mn *d*-hole count) across the entire series is supported by this plot. This correlation spans the break point near the $x=0.2$ composition as indicated by the points in the 3.84–3.88 Å range. Thus both the structural and XAS results seem consistent with the proposal that the Mn *d*-hole count of rhombohedral $LaMnO_3$ is initially somewhat decreased by Ca substitution with a large *d*-hole increase setting in only for $x>0.2$.

TABLE I. Unit-cell parameters of $La_{1-x}Ca_xMnO_3$ from x-ray powder-diffraction, least-squares fitting results. Some samples were refined in the closely related rhombohedral ($R\bar{3}c$) and pseudocubic ($Pm\bar{3}m$) structures. The effective reduced cubic perovskite cell lattice parameter (a_P) is presented (see Refs. 26 and 27) so that the effective lattice dilatation can be compared between structures.

x	a(Å) [for $Pm\bar{3}m$ & for $R\bar{3}c$]	α(°) [for $R\bar{3}c$]	a_p (Å)	Comment[a]
0.0	5.4679(8)	60.65(2)	3.8852(6)	RU
0.05	5.4616(5)	60.58(3)	3.8787(3)	RU
0.1	5.4620(1)	60.58(3)	3.8740(1)	RU
0.15	5.475(1)	60.09(3)	3.8790(1)	RU
0.2	5.488(1)	59.98(3)	3.8800(7)	RU
0.4	7.712(4)		3.884(1)	RU
0.6	7.623(2)		3.814(1)	RU
0.8	7.519(2)		3.753(3)	RU
1.0	7.4582(2)		3.7292(2)	RU
0.25	7.7498(8)		3.8749(4)	LT
0.35	7.704(3)		3.852(2)	LT
0.4	7.695(2)		3.848(1)	LT
0.5	7.658(1)		3.892(1)	LT
0.67	7.595(3)		3.7975(2)	LT
0.9	7.4925(8)		3.7463(4)	LT

[a]The sample prepared at Rutgers University (RU) or at Bell Labs, Lucent Technologies (LT).

$La_{1-x}Ca_xMnO_3$ OXYGEN ANNEALING RESPONSE

Previous studies of $LaMnO_3$ have attributed the apparent incorporation of excess O, and concomitant increase of Mn^{4+} concentration (as determined by titration), to metal (La and Mn) site vacancies.[7,9,24,25] Moreover, preparation conditions of the substituted Mn perovskites (both in bulk and in thin-film form) vary substantially in the literature. Therefore it was deemed worthwhile to investigate the Mn *K*-XAS response of selected samples (i.e., $x=0$, 0.2, 0.4, 0.6, 0.8, and 1.0) in the $La_{1-x}Ca_xMnO_3$ series to annealing in a pure O_2 atmosphere (24 h at 1100 °C). In Fig. 6(a) the Mn *K*-XAS spectra for air-prepared and O_2-annealed samples with $x=0$, 0.4, and 1.0 are shown. The spectra for O_2-annealed samples all manifested a shift to higher energy relative to the as-prepared samples, consistent with the O-induced creation of Mn *d*-holes. However, except for the $x=0.2$ and 0.4 compositions these shifts were small as indicated in Fig. 6(d). The greatest O response appeared to be at the $x=0.4$ composition with the $x=0.2$ composition response also being sizable but somewhat smaller.

These results indicate that the average Mn *d*-count response to O_2 annealing in these materials is not simple. In the high x regime the lack of available Mn^{3+} sites presumably limits the magnitude of this response. The small response of the $x=0$ material, on the other hand, may reflect it naturally has a higher relative O content with air sintering, so that the O anneal has little additional effect. Within this interpretation the higher response in the $x=0.2$ and 0.4 compositions could reflect a Ca-induced lowering of the effective

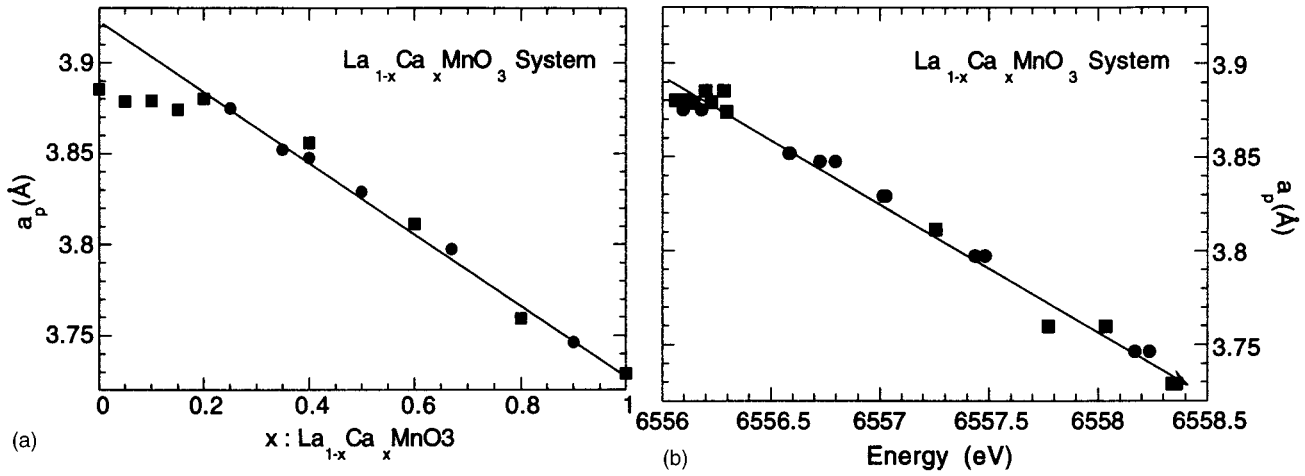

FIG. 5. (a) (left) The effective perovskite unit-cell parameter (see Refs. 26 and 27) versus Ca^{2+} concentration for the samples used in this study. The solid squares are the Rutgers (RU) samples and the solid circles are the Lucent Technology (LT) samples. (b) (right) The Mn K-edge peak position is plotted versus the effective perovskite unit-cell parameter for the samples in this study. Note the correlation across the series, including through the energy where the break in the compositional dependence was observed. Note also that multiple measurements at selected compositions have been included to indicate the experimental uncertainties.

O content in the air-prepared materials. The FM and charge ordering interactions could also play a role in the varying susceptibility of the Mn toward additional oxidation. Additional experimental work is planned to address these issues.

CONCLUSIONS

Mn K-edge XAS measurements presented here mandate a large Mn d-hole increase (h_d), with increasing x, across the $La_{1-x}Ca_xMnO_3$ series of compounds. Within the limitations of comparison to pure oxide standards the net variation in h_d is consistent with the loss of about $0.7e^-$ between the end-point compounds ($x=0.0$ and 1.0). Moreover, the XAS results presented here have been interpreted in terms of a picture in which h_d increases nearly linear from $x\approx0.2$ to $x=1.0$, but in which there is also very little change in h_d between $x=0.0$ and $x\approx0.2$.

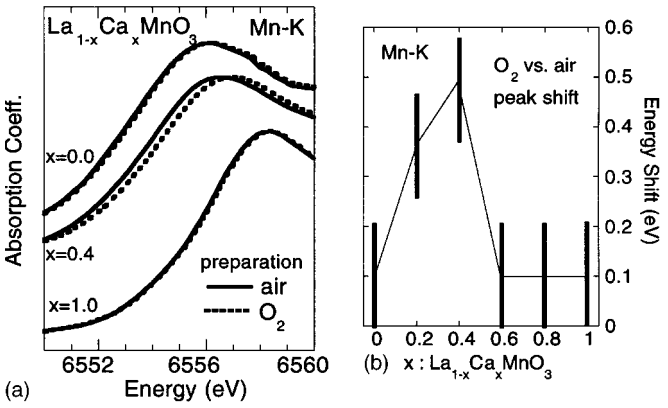

FIG. 6. (a) (left) The Mn K-edge spectra for the $x=0.0$, 0.4, and 1.0 samples in the $La_{1-x}Ca_xMnO_3$ series with differing preparation. The solid line spectra are for as-prepared (in air) samples and the dotted line spectra are for O_2-annealed samples. Note the larger shift to higher energy of the O_2-annealed $x=0.4$ spectrum with respect to the as-prepared spectrum. (b) (right) The difference in the energy of the B-feature peak, for air-synthesized and O_2-annealed samples, versus composition in the $La_{1-x}Ca_xMnO_3$ series. The heavy solid lines indicate the experimental uncertainties and the light line is a guide to the eye. Note the increased response at the 0.2 and 0.4 compositions.

In the physical properties of the $La_{1-x}Ca_xMnO_3$ series the $x\approx0.2$ composition is a watershed marking: the onset of metallic behavior; the onset of a rapid rise of the FM ordering temperature (with increasing x); and the crystal structure change from rhombohedral to cubic.[1–3] That the Mn K-XAS results should mirror these changes is perhaps not surprising. Although structural or magnetic origins of the observed Mn K-XAS changes should not be excluded, the conventional interpretation of the Mn d-count origin has been followed here. Within this viewpoint the Mn d-count variation coupling to the other physical properties must be considered.

The metallic conduction and FM double exchange in these materials is based on the introduction of holes in the Mn e_g states (of the $Mn^{3+}t_{2g}^3e_g^1$ configuration) thereby forming Mn^{4+} t_{2g}^3 configuration sites.[1–3,5] Our results support the notion that the e_g hole formation (with Ca substitution) does not open up until $x\approx0.2$. Whether the e_g hole formation in the $x<0.2$ range is arrested by a greater O p-hole character or whether a more complicated x variation in the O/metal stoichiometry is operative is not presently clear. However, within the present interpretation the magnetic and metallization changes (onsetting near $x\approx0.2$) would coincide with the onset of the strong Mn $d(e_g)$ hole response to Ca substitution. As noted in the text, selected previous spectroscopic results have at least hinted at a break in the electronic structure in this composition range.[16,17]

As suggested above, the issue of the O stoichiometry and metal-site vacancy variation, as a function of x, needs to be kept in mind for further studies. Specifically the lack of Mn d response, at low x, could involve a reduction in the effective O to metal content, induced by the Ca substitution.

Whatever the detailed cause, the XAS results should still be representative of the air-synthesized materials used in most systematic studies of this system. Summarizing then, for such materials the XAS results support the notion that the Mn d (presumably e_g) hole response to A^{2+} substitution is delayed in composition to $x \approx 0.2$. This proposal clearly must be examined both theoretically and experimentally before definite conclusions can be drawn. However, the correlation of the rapid rise in the FM ordering temperature and metallic-behavior onset, within this view, with the onset of the Ca-induced $d(e_g)$-hole formation is strongly suggestive.

ACKNOWLEDGMENTS

The authors would like to acknowledge L. Dyibo and N. Croft for assistance in the XAS data collection, and P. Ansari for helpful discussions. This work was supported in part by the NSF under DMR 95-01504, and NSF Solid State Chemistry Grant No. DMR 93-14605.

[1] P. Schiffer, A. Ramirez, W. Bao, and S.-W. Cheong, Phys. Rev. Lett. **75**, 3336 (1995).

[2] A. Ramirez, P. Schiffer, S.-W. Cheong, C. H. Chen, W. Bao, T. T. M. Palstra, B. Zegarski, P. L. Gammel, D. J. Bishop, and B. Zegarski, Phys. Rev. Lett. **76**, 3188 (1996).

[3] A. Urushibara, Y. Moritomo, T. Arima, A. Asamitsu, G. Kido, and Y. Tokura, Phys. Rev. B **51**, 14 103 (1995).

[4] S. Jin *et al.*, Science **264**, 413 (1994); R. von Helmolt *et al.*, Phys. Rev. Lett. **71**, 2331 (1993); K. Chahara *et al.*, Appl. Phys. Lett. **63**, 1990 (1993); R. M. Kusters *et al.*, Physica B **155**, 362 (1989).

[5] C. Zener, Phys. Rev. **82**, 403 (1951); P. G. De Genes, *ibid.* **118**, 1413 (1960).

[6] A. Millis, P. B. Littlewood, and B. B. Shraiman, Phys. Rev. Lett. **74**, 5144 (1995).

[7] J. van Roosmalen, P. Vlaanderen, and E. Cordfunke, W. IJduo, and D. IJdo, J. Solid State Chem. **114**, 516 (1995).

[8] G. H. Jonker and J. H. van Santen, Physica **16**, 337 (1950); J. H. van Santen and G. H. Jonker, *ibid.* **16**, 559 (1950).

[9] R. Mahendiran, S. Tiwary, A. Raychaudhuri, T. Ramakrishnon, R. Mahesh, N. Rangavittal, and C. N. R. Rao, Phys. Rev. B **53**, 3348 (1996).

[10] See, N. Nucker *et al.*, Phys. Rev. B **37**, 5158 (1988).

[11] J. Tranquada, S. Heald, A. Moodenbaugh, G. Liang, and M. Croft, Nature (London) **337**, 720 (1989).

[12] Z. Tan, S. Heald, S.-W. Cheong, A. Cooper, and A. Moodenbaugh, Phys. Rev. B **47**, 12 365 (1993).

[13] A. Shainer, M. Croft, S. Guha, I. Perez, Z. Zhang, M. Greenblatt, P. Metcalf, H. Jhans, and G. Liang, Phys. Rev. B **51**, 5879 (1995).

[14] A. Shainer, M. Croft, Z. Zhang, M. Greenblatt, I. Perez, P. Metcalf, H. Jhans, G. Liang, and Y. Jeon, Phys. Rev. B **53**, 9745 (1996).

[15] M. Abbate, F. de Groot, J. Fuggle, A. Fujimori, O. Strrebel, F. Lopez, M. Domke, G. Kaindl, G. Sawatzky, M. Takano, Y. Takeda, H. Eisaki, and S. Uchida, Phys. Rev. B **46**, 4511 (1992).

[16] T. Saitoh, A. Bocquet, T. Mizokawa, H. Namatame, A. Fujimori, M. Abbate, Y. Takeda, and M. Takano, Phys. Rev. B **51**, 13 942 (1995).

[17] D. Samara, O. Rader, T. Kachel, A. Chainani, M. Mathew, K. Holldack, W. Gudat, and W. Eberhardt, Phys. Rev. B **49**, 14 238 (1994).

[18] J.-H. Pak, C. T. Chen, S.-W. Cheong, W. Bao, G. Megs, V. Chakarian, and Y. U. Idzerda, Phys. Rev. Lett. **76**, 4215 (1996).

[19] R. J. H. Voorhoeve, D. W. Johnson, J. P. Remaika, and P. K. Gallaghar, Science **195**, 827 (1977).

[20] T. Guo and M. denBoer, Phys. Rev. B **31**, 6233 (1984).

[21] See, *X-ray Absorption: Principles, Applications, Techniques of EXAFS and SEXAFS, and XANES*, edited by D. Koningsberger and R. Reins (Wiley, New York, 1988).

[22] S. Cramer *et al.*, J. Am. Chem. Soc. **98**, 1287 (1976); P. Sarode *et al.*, J. Phys. C **12**, 2439 (1979); M. Belli *et al.*, Solid State Commun. **35**, 355 (1980).

[23] See Refs. 13 and 14 and references therein for examples of such pre-edge and $4p$ features. Also note, for a specific example, in Ref. 13 the Ni K-edge work on the $La_{2-x}Sr_xNiO_4$ system. In that system the initial Ni K-edge onset governed by the variation of the out-of-plane Ni $4p_\pi$ final state, and the main peak by the in-plane Ni $4p_\sigma$ final state. With increasing x, in that system, the $4p_\pi$-$4p_\sigma$ energy splitting systematically decreases.

[24] R. Mahesh, R. Mahendiran, A. Raychaudhuri, and C. N. R. Rao, J. Solid State Chem. **114**, 297 (1995).

[25] R. Mahesh, K. Kannan, and C. N. R. Rao, J. Solid State Chem. **114**, 294 (1995); J. van Roosmalen, P. van Vlaanderen, E. Cordfunke, W. IJdo, and D. IJdo, *ibid.* **114**, 516 (1995).

[26] For the rhombohedral cell volume see B. Cullity, *Elements of X-Ray Diffraction* (Addison-Wesley, Reading, MA, 1967), p. 460. Note also, as discussed in Refs. 24 and 25, that the cubic cell dimension is simply doubled with respect to the perovskite containing four formula units; and the rhombohedral cell is formed along the body diagonal of the doubled cubic structure containing two formula units.

[27] For use of the effective perovskite cell parameter, see F. Galasso, *Structure, Properties and Preparation of Perovskite-Type Compounds* (Pergamon, New York, 1969), p. 143.